research papers

Accurate dosimetry in scanning transmission X-ray microscopes *via* the cross-linking threshold dose of poly(methyl methacrylate)

Adam F. G. Leontowich,[a]* Adam P. Hitchcock,[a] Tolek Tyliszczak,[b] Markus Weigand,[c] Jian Wang[d] and Chithra Karunakaran[d]

[a]Brockhouse Institute for Materials Research, McMaster University, 1280 Main Street West, Hamilton, Ontario, Canada L8S 4M1, [b]Advanced Light Source, Lawrence Berkeley National Laboratory, One Cyclotron Road, MS 6R2100, Berkeley, CA 94720, USA, [c]Max Planck Institute for Intelligent Systems, Stuttgart, Baden-Württemberg 70569, Germany, and [d]Canadian Light Source Inc., 101 Perimeter Road, Saskatoon, Saskatchewan, Canada S7N 0X4.
E-mail: leontoaf@mcmaster.ca

The sensitivity of various polymers to radiation damage by soft X-rays has been measured previously with scanning transmission X-ray microscopes. However, the critical dose values reported by different groups for the same material differ by more than 100%. Possible sources of this variability are investigated here for poly(methyl methacrylate) (PMMA) using controlled exposure to monochromatic soft X-rays at 300 eV. Radiation sensitivity, judged by several different criteria, was evaluated as a function of dose rate, pre-exposure thermal treatments and X-ray polarization. Both the measured critical dose and the dose required to initiate negative mode (cross-linking) were observed to depend only on dose, not the other factors explored. A method of determining detector efficiency from the dose required to initiate negative mode in PMMA is outlined. This method was applied to many of the soft X-ray STXMs presently operating to derive the efficiencies of their transmitted X-ray detectors in the C 1s absorption-edge region.

Keywords: poly(methyl methacrylate); STXM; radiation damage; dosimetry; detector efficiency.

1. Introduction

Many advanced technologies use ionizing radiation as a processing tool. In these applications, knowledge of the radiation sensitivity [the absorbed dose required to produce a defined outcome, following the Grotthuss–Draper law (King & Laidler, 1984)] of materials is critical. For example, polymer thin films or resists are irradiated and used as sacrificial layers in the manufacture of integrated circuits. The sensitivity of a resist is an important characteristic when considering its suitability for a specific manufacturing process. Assuming all other processing properties are equal, a more sensitive resist, *i.e.* one which requires less dose to reach the same outcome, would increase productivity. The dose accuracy when measuring radiation sensitivity is therefore of critical importance. In proton therapy, beams of energetic protons are used to destroy cancerous tissues (Hall & Giaccia, 2006). The goal is to destroy the offensive tissue using the minimum dose possible to limit the destruction of the surrounding healthy tissue, therefore the accuracy of the radiation dose administered is of utmost importance. For dose-dependent applica-

tions of ionizing radiation, the precision and accuracy of dose determinations are critical to achieving reproducible outcomes across the field of radiation science.

Several studies involving radiation damage to polymer thin films have been carried out using scanning transmission X-ray microscopes (STXMs) (Zhang *et al.*, 1995; Coffey *et al.*, 2002; Beetz & Jacobsen, 2003; Wang *et al.*, 2007, 2009a,b). In these studies the sensitivity is often reported in terms of a critical dose, or the absorbed dose required to cause a decrease (or increase) in the intensity of a chosen spectroscopic feature to 1/e or 37% of its initial value. Although the methodology is seemingly quite similar, there is frequently relatively poor agreement among critical dose values derived for nominally the same material and spectral feature, with values in some cases differing by more than 100%. Reported critical dose values for the decrease of the C $1s$(C=O) $\rightarrow \pi^*_{C=O}$ signal (288.4 eV) of poly(methyl methacrylate) (PMMA) measured by STXMs differ by more than 500% (Zhang *et al.*, 1995; Coffey *et al.*, 2002; Wang *et al.*, 2007, 2009a). It is puzzling why the goal of deriving what should be a fundamental property of a material has so far been elusive to STXM microscopists.

PMMA-based radiation dosimeters for the 0–100 kGy dose region are commercially available (Red 4034, Amber 3042, Harwell Dosimeters) and have been in use for several decades (Barrett, 1982). They are commonly used in industrial radiation processing applications such as the sterilization of medical devices and the processing of foods. Once critical control parameters are understood and protocols are established, dose can be measured very accurately. There are several possibilities that may explain the discrepancies in the literature. Dose rate has been shown to affect radiation sensitivity using electrons (Jiang & Spence, 2012), ions (Schrempel & Witthuhn, 1997) and high-energy photons (Plaček et al., 2003; Leiros et al., 2006). The possible influence of dose rate for the STXM studies cited above was acknowledged by some (Coffey et al., 2002; Wang et al., 2009a) but not further investigated. Pre-exposure thermal treatments could also play a role, as was suggested by Zhang et al. (1995).

In this report PMMA is used as an example of a radiation-sensitive material, and several factors which could explain why accurate radiation sensitivity quantitation has been a challenge for STXMs are examined. First, pre-exposure thermal treatments, dose rate and X-ray polarization were systematically varied while the effects on the radiation damage characteristics of PMMA as a function of dose were measured by a combination of lithographic techniques, atomic force microscopy (AFM) and near-edge X-ray absorption fine-structure (NEXAFS) spectroscopy. The dose for the onset of negative mode (cross-linking) was found to be very reproducible, and independent of the factors investigated. A facile method to determine the efficiency of a STXM X-ray detector involving the onset of negative mode is presented. This measurement was then carried out at most of the currently operational soft X-ray STXMs. Large differences were found among the detector efficiencies of different STXMs, which may account for much of the variation in critical dose values reported in previous studies.

2. Methodology

2.1. Materials

PMMA (electronics grade, M_w = 315000, M_w/M_n = 1.05, synthesized by living anionic polymerization, sec-butyllithium initiator) was purchased from Polymer Source. Toluene 99.9% Chromasolv and 4-methyl-2-pentanone (MIBK) >98.5% ACS reagent grade were purchased from Sigma-Aldrich. 2-Propanol (IPA) 99.5% was purchased from Caledon Laboratories. Mica was purchased from Ted Pella. Si_3N_4 windows (75 nm × 1 mm × 1 mm window in a 200 μm × 5 mm × 5 mm Si wafer frame) were purchased from Norcada. All materials were used as received.

2.2. Sample preparation

Thin films of PMMA were fabricated by spin casting four drops of a 1.5% w/w PMMA/toluene solution onto a 1.5 cm × 1.5 cm piece of freshly cleaved mica. The films remained in ambient air for 10 min and were then cut into 3 mm × 3 mm

pieces with a scalpel. Upon slowly dipping the mica into a Petri dish filled with distilled water, small pieces of the film release and float on the water's surface. These were then caught on Si_3N_4 windows in an orientation such that the film only partially covered the window to allow for measurements of the incident X-ray flux (I_0) in the bare regions. Samples labelled 'as-spun' underwent no further processing. Samples labelled 'vacuum dried' were placed in a vacuum oven (2×10^{-2} torr) at 343 K for 24 h. Samples labelled 'annealed' were placed on a hot plate at 423 K for 1 h. Temperatures were monitored using a K-type thermocouple and a glass thermometer (±1 K). The film thicknesses were 50 ± 5 nm, measured by AFM across a scratch through the film, and by STXM by dividing the measured optical density (OD) in the C 1s region by the response of 1 nm of PMMA, established by matching the C 1s NEXAFS spectrum of PMMA between 275–282 eV and 340–360 eV to the absorption predicted from the literature elemental X-ray absorption coefficients (Henke et al., 1993) for $C_5H_8O_2$, and the bulk density of PMMA (1.18 g cm^{-3}). Thickness values from both techniques were in agreement within 5%.

2.3. Development

The sample was held with locking tweezers and gently stirred in a vial containing a 3:1 v/v solution of IPA:MIBK for 30 s, then immediately stirred in a waiting vial of IPA for 15 s. The sample was then allowed to dry in air. Development and air drying occurred at ambient temperature (293–298 K).

2.4. Scanning transmission X-ray microscope

Five soft X-ray (80–2500 eV) STXMs were used to expose PMMA samples to 300 eV X-rays and to probe the irradiated material after exposure. The instruments used were located at the following beamlines: 5.3.2.2 (Kilcoyne et al., 2003) and 11.0.2 (Tyliszczak et al., 2004) at the Advanced Light Source [ALS; Lawrence Berkeley National Laboratory, Berkeley (LBNL), USA]; 10ID-1 (Kaznatcheev et al., 2007) at the Canadian Light Source (CLS; Saskatoon, Canada); X07DA (Raabe et al., 2008) at the Swiss Light Source (SLS; Paul Scherrer Institute, Villigen, Switzerland); and UE46 (Follath et al., 2010) at Berliner Elektronenspeicherring-Gesellschaft für Synchrotronstrahlung (BESSY II; Berlin, Germany). Henceforth the individual instruments will be referenced by the beamline at which they presently reside. While the beamlines differ, all five of these STXMs are essentially based on the ALS 5.3.2.2 design (Kilcoyne et al., 2003) which is now commercially available (Bruker Advanced Supercon GmbH, formerly Accel). All are equipped with precise in-vacuum piezo shutter systems which can reliably go from closed to open to closed in 1 ms (Kilcoyne & Tyliszczak, 2004). At present all of these STXMs use the same operational software, STXM_Control (Kilcoyne et al., 2003). All maintain the sample position (x, y) relative to the zone plate lens to better than 10 nm by laser interferometer feedback systems. For these experiments all were equipped with zone plates with the same characteristics (25 nm outer most zone width, 240 μm

Adam F. G. Leontowich et al. • Accurate dosimetry in STXMs

research papers

diameter, 90 µm central stop) from the Center for X-ray Optics, LBNL. Except for UE46, the transmitted X-ray detectors consist of a phosphor scintillator to convert soft X-rays to visible-wavelength photons which are then counted by a high-performance photomultiplier tube (PMT) (Kilcoyne *et al.*, 2003; Fakra *et al.*, 2004). At UE46 the X-rays were detected directly using an avalanche photodiode (S2382, Hamamatsu) gated to the arrival times of the 500 MHz flashes of synchrotron light to reduce background.

Samples were fixed to an aluminum sample plate and loaded into the STXM chamber. The chamber was evacuated to 0.1 torr by pumping for about 10 min, then backfilled with 250 torr He. The evacuation step is important because O_2 has been shown to affect the radiation damage chemistry of thin polymer layers (Coffey *et al.*, 2002). All possible efforts were taken to eliminate higher order radiation. Higher order X-rays were blocked geometrically by the sufficiently absorbing central stop incorporated in the zone plate, and an order-sorting aperture (OSA), carefully centered on the optical axis. The OSA diameter and OSA-to-sample distances were chosen to select only the zone plate first order component. In addition, higher order suppression systems were used on beamlines that currently have them [a 200 nm Ti foil at 10ID-1, a 1.0 m-long section of the beamline differentially pumped with N_2 at 600 mtorr at 5.3.2.2, and a MgF_2-coated mirror system at X07DA (Frommherz *et al.*, 2010)]. The detector was positioned so that the active area accepted the entire transmitted bright field signal. The photon energy scales were calibrated to an accuracy of 0.05 eV using the known C $1s(C{=}O) \rightarrow \pi^*_{C=O}$ peak of PMMA at 288.45 eV (Wang *et al.*, 2007). Photon energy scale shifts during a set of measurements over a few days at any given beamline were less than 0.1 eV.

2.4.1. Imaging and spectroscopy. STXMs focus monochromatic X-rays into an intense 30 nm-diameter spot [Rayleigh criterion for a 25 nm outer most zone width zone plate operated under diffraction-limited conditions (Howells *et al.*, 2007)]. Samples are then positioned at the focal plane and *x–y* raster scanned through the X-ray spot under computer control while the transmitted signal is acquired to form transmission images at X-ray photon energies. These transmission images can be converted to OD images by applying the Lambert–Beer law with an I_0 measurement through a suitable blank. In addition, NEXAFS spectra can be measured by recording image sequences, or 'stacks' (Jacobsen *et al.*, 2000), over a photon energy range of interest. If necessary, the images were aligned spatially using Fourier-transform-based cross-correlation procedures. The resulting data set (*x*, *y*, *E*) provides a NEXAFS spectrum at each pixel. The detailed procedures for imaging, spectroscopy and data analysis have been reviewed elsewhere (Jacobsen *et al.*, 2000; Ade & Hitchcock, 2008; Hitchcock, 2012). Image and spectroscopic data processing was performed using the program *aXis2000*.

2.4.2. Patterning. Samples were precisely patterned using PatternGen, a routine within *STXM_Control*. The pattern-generation input files (*.xyt) consist of a set of records, with

each record providing the *x–y* positional coordinates for each point exposure and the length of time the piezo shutter is to be opened. The input file used for all experiments here consisted of nine 600 nm × 600 nm areas, each composed of 10 × 10 single point exposures with a pitch of 60 nm (see Fig. 1 of the supplementary material), and each area has a progressively increasing exposure time. This input file and instructions for creating such files are included as supplementary material.[1] In order to obtain reproducible results it is necessary to set the microscope to best focus before executing the pattern, which can be achieved using a micrometer or sub-micrometer specimen of radiation-insensitive material in/on the sample, which is typically a piece of mica from sample preparation. The focus must be set within a few tens of micrometers of the patterned area, as it is not currently possible to reliably have the sample perfectly orthogonal to the X-ray beam over much more than 80 µm. Care was taken during set-up so that the areas of the sample to be patterned were never imaged with the STXM, as even a single image with typical microscope settings can cause quantifiable radiation-induced effects (supplementary Fig. 2). When the pattern-generation scan is initiated, the program performs the following sequence: (i) with the shutter closed, move to the desired position (*x*, *y*) under interferometric feedback, (ii) open the shutter, (iii) close the shutter after the specified exposure time for that point. This sequence is repeated for each record in the input file until all points have been exposed. Patterning in this way is very accurate, precise and reproducible. The temperature of the aluminum sample plate during patterning was monitored with a K-type thermocouple bonded 2 mm from the sample, and was found to be 298 ± 2 K.

In order to determine dose, I_0 at the patterning photon energy must be measured immediately before and/or after patterning. It is critical to measure I_0 with exactly the same parameters used for patterning, *i.e.* no refocusing, no changes in slit settings, no changes to the OSA position, *etc.* The CLS (10ID-1) and BESSY II (UE46) synchrotrons were operating in multi-bunch mode when these experiments were performed. For those measurements, I_0 was measured before and after each pattern was executed, and the average value was used. As the total time to execute the nine area patterns is 5–10 min, the before–after difference was never more than 3%. The SLS (X07DA) and ALS (5.3.2.2, 11.0.2) operated in top-up mode so the storage ring current and thus the X-ray flux through the shutter was constant (to within 0.2%); only one I_0 measurement was necessary.

2.4.3. Calculating dose. Absorbed dose (amount of energy absorbed by the sample volume divided by the amount of mass irradiated) *D* was calculated using the following equation,

$$D = (F/K)\,t\,E/Vd \tag{1}$$

where *D* is the dose in Grays (Gy = J kg^{-1}); *F* is the photon absorption rate of the irradiated volume of material (photons

---

[1] Supplementary data for this paper are available from the IUCr electronic archives (Reference: HF5212). Services for accessing these data are described at the back of the journal.

s^{-1}) at the chosen patterning photon energy; K is the detector efficiency (unitless), which is the ratio of the number of single photon events per second counted, over the photons s^{-1} that impinge on the detector, and must be determined experimentally at the photon energy of exposure. At 5.3.2.2, K was determined by comparing the PMT signal with that from a calibrated Si photodiode (AXUV-HS1; International Radiation Detectors) and found to be 35 ± 5% at 300 eV; t is the exposure time (s); E is the energy per photon (J photon^{-1}) at the patterning photon energy (300 eV throughout this work); V is the volume of the material irradiated (cm^3), in this case the exposure area multiplied by the film thickness; d is the density of the material (1.18 g cm^{-3} for PMMA).

If the X-ray absorption cross section at the patterning photon energy does not change significantly as a function of dose (which must be determined experimentally, but is often valid for very short exposures, highly radiation-resistant materials, and materials which do not undergo mass loss with increased dose) the photon absorption rate is simply the difference between I_0 and I, the photons s^{-1} transmitted through the sample,

$$F = I_0 - I. \tag{2}$$

This approach is valid in the photon energy region currently accessible with soft X-ray STXMs (80–2500 eV) where photoabsorption dominates over all other process by orders of magnitude for most elements [three orders of magnitude for carbon (Hubbell *et al.*, 1980)] and it can be safely assumed that F is due to photoabsorption alone. A convenient form of the photon absorption rate for STXMs is (derivation in the supplementary material),

$$F = I_0[1 - \exp(-OD)] \tag{3}$$

where OD is the optical density of the polymer film at the patterning photon energy, measured from an OD image recorded adjacent to the patterning area. These values depend on the individual beamlines and the response of the material at specific photon energies and must be determined experimentally.

It is often the case, however, that irradiation induces chemical change, mass loss, *etc.*, which results in changes to the X-ray absorption cross section of a material as a function of dose. F is then not constant, and the changes in F during exposure must be accommodated when determining the dose. For several polymers including PMMA, the change in absorption cross section as a function of dose has been experimentally determined to follow first-order rate laws (Zhang *et al.*, 1995; Coffey *et al.*, 2002; Beetz & Jacobsen, 2003; Wang *et al.*, 2007, 2009a,b). Specifically, when the X-ray absorption features decay exponentially to a residual value, the following applies,

$$OD = OD_\infty + a\exp(-bt) \tag{4}$$

where OD is the OD of the polymer film after exposure time t, OD_∞ is the residual OD value of the polymer film after receiving a very high dose, and a and b are found through a fit to the data points by plotting OD as a function of t. To compute absorbed dose in cases where the X-ray absorption cross section at the patterning photon energy undergoes exponential decay in response to dose as the patterning proceeds, the OD term in (3) is replaced by the integrated OD at the patterning photon energy for a given exposure time,

$$OD = \frac{\int_0^t [OD_\infty + a\exp(-bt)]\, dt}{t}$$
$$= \frac{OD_\infty t + (a/b)[1 - \exp(-bt)]}{t}. \tag{5}$$

As PMMA is irradiated, it undergoes mass loss, which results in the exponential decay of the X-ray absorption cross section at 300 eV. Therefore, the integrated OD [equation (5)] was used in this work. Doses were calculated using an Excel spreadsheet, which is available upon request.

2.5. Other characterization techniques

Thermogravimetric analysis was performed with a Netzsch STA 409 PC/PG thermal analyser. Optical micrographs were collected with an Olympus BX51 optical microscope equipped with a 100× objective and a CCD camera. AFM was performed using a Quesant Q-Scope 350 microscope with Budget Sensors Tap 150 Al-G probes in intermittent contact mode with a 0.5 Hz scan rate.

3. Results

3.1. Thermal characterization of PMMA

Thermogravimetric analysis was performed on PMMA in as-received powdered form measured in air with a temperature ramp of 5 K min^{-1} (Fig. 1). The glass transition (T_g) occurred at 376 K while thermal degradation (T_d) took place at and above 503 K.

3.2. Surface roughness of PMMA films

Atomic force micrographs were taken of the as-spun, vacuum-dried and annealed samples. RMS roughness values were determined from these micrographs and are presented
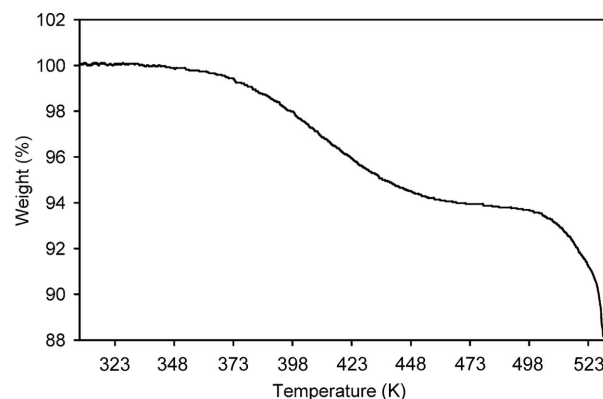

Figure 1
Thermogram of as-received powdered PMMA in air. Ramp rate: 5 K min^{-1}.

research papers

Table 1
Effect of thermal treatments on the surface roughness of PMMA as measured from atomic force micrographs.

Sample	RMS roughness (nm)
As-spun	0.78
Vacuum dried (343 K, 2×10^{-2} torr, 24 h)	1.08
Annealed (423 K, 1 h)	0.70

in Table 1. The annealed samples showed the lowest RMS roughness relative to the as-spun and vacuum-dried samples.

3.3. Patterning

As-spun, vacuum-dried and annealed samples were loaded into 5.3.2.2 and patterned using the input file described in §2.4.2. After patterning, the samples were removed from the STXM and inspected with an optical microscope (Fig. 2a). All nine patterned areas are resolved, and they become increasingly transmissive with increasing dose. An atomic force micrograph of the patterned areas is presented in Fig. 2(b). The individual exposures which make up each area are resolved in detail. The heights of individual patterned areas were measured and plotted versus dose (Fig. 2c). The height of the PMMA film decreased with increasing dose roughly linearly until 60 ± 15 MGy, at which point the film thickness was
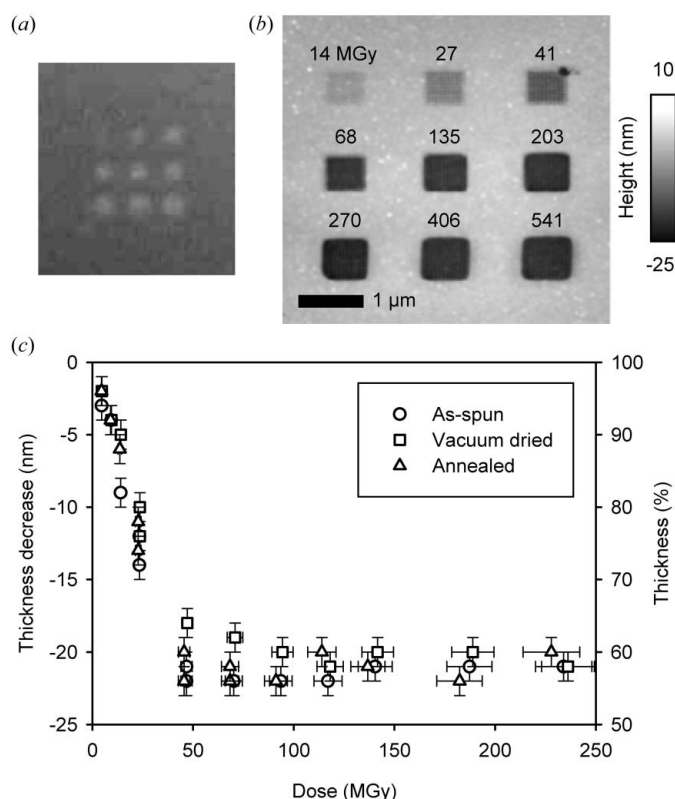

Figure 2
(a) Optical micrograph (transmission, $100\times$) of an annealed PMMA sample after patterning with 300 eV X-rays. (b) Atomic force micrograph of PMMA after exposure [same area/doses for (a) and (b)]. (c) Plot of the height reduction of individual patterned areas versus dose. Results from different pre-exposure thermal treatments [as-spun, vacuum-dried (343 K, 2×10^{-2} torr, 24 h) and annealed (423 K, 1 h)] are compared.

reduced by 40%. No significant height changes were observed for doses beyond this point up to 900 MGy, as long as carbon contamination was not significant (§4.4). This behavior was found to be independent of the different pre-exposure thermal treatments and dose rate over the 73–1230 MGy s^{-1} range investigated, accomplished by adjusting the monochromator exit-slit widths (increasing/decreasing I_0) and t.

3.4. Spectromicroscopy

Spectroscopic changes within the patterned areas were investigated with 5.3.2.2. Stacks of the patterned areas were collected, and C 1s NEXAFS spectra of individual patterned areas were obtained by extracting the average spectrum of the central region of each area (roughly 400 nm $\times$ 400 nm). The dose associated with the stack acquisition was 5–10 MGy. Spectra corresponding to four different doses are compared in Fig. 3. Several spectral changes were observed as the dose increases. A new feature at 285.1 eV attributed to C=C bond creation appears and increases with dose. The signal intensity at 288.4 eV, corresponding to the C 1s(C=O) $\rightarrow$ $\pi^*_{C=O}$ decreases with dose, as does the C 1s continuum signal ($\geq$305 eV). The signal at 305 eV was reduced by 30% relative to the virgin polymer after receiving 150 MGy. These observations are consistent with other NEXAFS investigations of PMMA (Zhang et al., 1995; Coffey et al., 2002; Wang et al., 2007, 2009a). In this work the spectral trends versus dose were investigated for the different pre-exposure thermal treatments noted and several dose rates between 73 and 1230 MGy s^{-1}. The spectral behavior in all cases was found to be identical given identical dose.

The integrated area of the 288.4 eV peak (above a background estimated as the average of the spectral intensities at 288.0 eV and 289.5 eV) is proportional to the number of C=O bonds in the volume sampled. Thus, a decrease of this peak is proportional to the amount of C=O bond loss or chemical change. OD images of several areas of as-spun, vacuum-dried
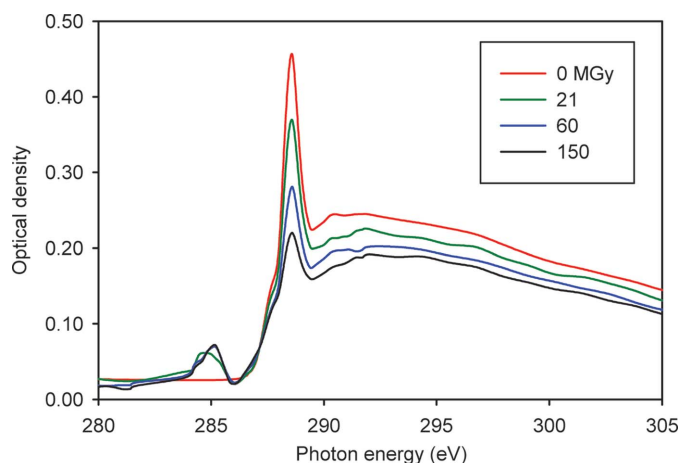

Figure 3
C 1s NEXAFS spectra of PMMA extracted from individual areas patterned with different doses of 300 eV X-rays (color online): 0 MGy (red), 21 MGy (green), 60 MGy (blue), 150 MGy (black). The spectral trends were observed to be independent of the pre-exposure thermal treatments noted and dose rate (73–1230 MGy s^{-1}).
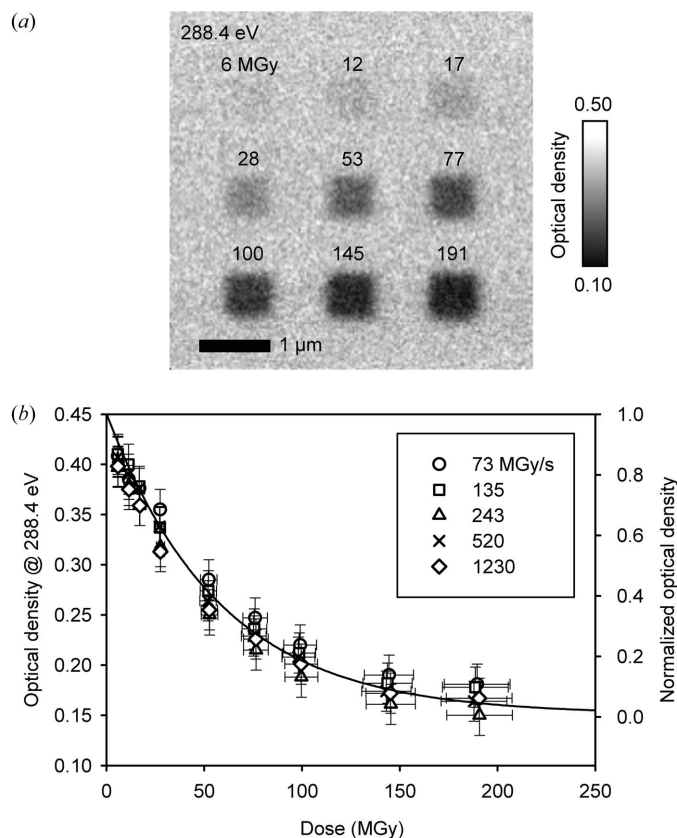
(a)

(a)

(b)

(b)

Figure 4
(a) STXM OD image (288.4 eV) of an annealed PMMA sample patterned with various doses of 300 eV X-rays. (b) Plot of the OD at 288.4 eV values of individual patterned areas *versus* dose for different dose rates ranging from 73 to 1230 MGy s^{-1}. In each case the OD at 288.4 eV exponentially decreases with a critical dose of 62 ± 8 MGy derived from the indicated fit (solid line) to the average of all data sets. The separate data sets all agree within measurement uncertainty.

Figure 5
(a) Atomic force micrograph of developed annealed PMMA showing several 600 nm × 600 nm areas patterned with various doses of 300 eV X-rays. (b) Measured heights of several 'cross-linked' PMMA areas plotted *versus* dose for as-spun, vacuum-dried (343 K, 2 × 10^{-2} torr, 24 h) and annealed (423 K, 1 h) samples.

and annealed samples patterned with different doses were collected with STXM 5.3.2.2 at 288.4 eV [an example image is shown in Fig. 4(a)]. The dose associated with collecting these OD images was less than 1 MGy. Average OD values of the central regions of many individual patterned areas were determined, and then plotted *versus* dose (Fig. 4b). These data were used to calculate the critical dose for the C 1s(C=O) → $\pi^*_{C=O}$ decrease at 288.4 eV. The critical dose was found to be 62 ± 8 MGy (average of the critical doses derived independently for each measurement; the uncertainty is the standard deviation). This result was independent of the pre-exposure thermal treatments noted and also independent of dose rate over the 73–1230 MGy s^{-1} range investigated.

3.5. Development

Some of the samples were subjected to development (§2.3) after patterning. An atomic force micrograph of developed annealed PMMA which was patterned at 5.3.2.2 is presented in Fig. 5(a). Doses greater than 1 MGy result in the full removal of the irradiated material by the developer, *i.e.* positive mode, while no measurable difference in the thickness of the non-patterned film away from the patterned areas was observed.
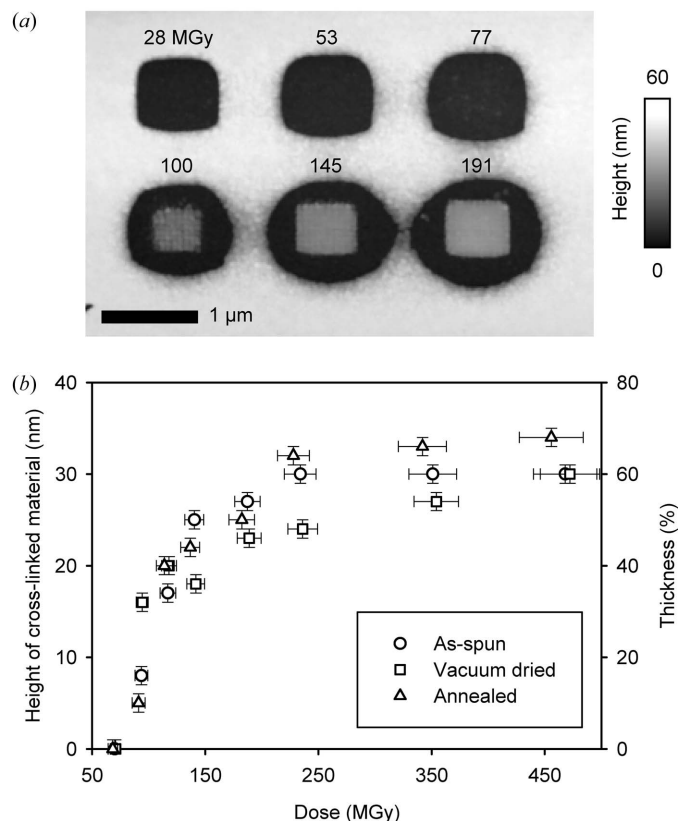
At a dose of 90 ± 4 MGy, PMMA switches from positive mode to negative mode, *i.e.* the irradiated material remains after development (Leontowich & Hitchcock, 2011). The height of this 'cross-linked' PMMA remaining in the patterned areas after development was measured for as-spun, vacuum-dried and annealed samples and the values were plotted *versus* dose (Fig. 5b). As the dose increases beyond the 90 ± 4 MGy onset of negative mode, the height of cross-linked PMMA increases and eventually reaches a maximum value near 350 MGy. The maximum height of the cross-linked PMMA corresponds to about 60% of the original film thickness. No further height changes were observed for doses from 350 to 900 MGy, as long as carbon contamination was not significant (§4.4). This behavior, and the onset of negative mode dose, was found to be independent of (i) pre-exposure thermal treatments; (ii) dose rate over the 73–1230 MGy s^{-1} range investigated; and (iii) X-ray polarization [left circular, right circular, 80% linear (circular polarized experiments were performed with 11.0.2)]. The individual 600 nm × 600 nm areas of cross-linked PMMA are large and dense enough to be resolvable in an optical microscope with a 50× or greater magnification objective lens (Figs. 6a, 6b). Although the as-spun, vacuum-dried and annealed samples required the same dose for the onset of negative mode and exhibit the same dose-dependent cross-linked material growth behavior (Fig. 5b), differences were
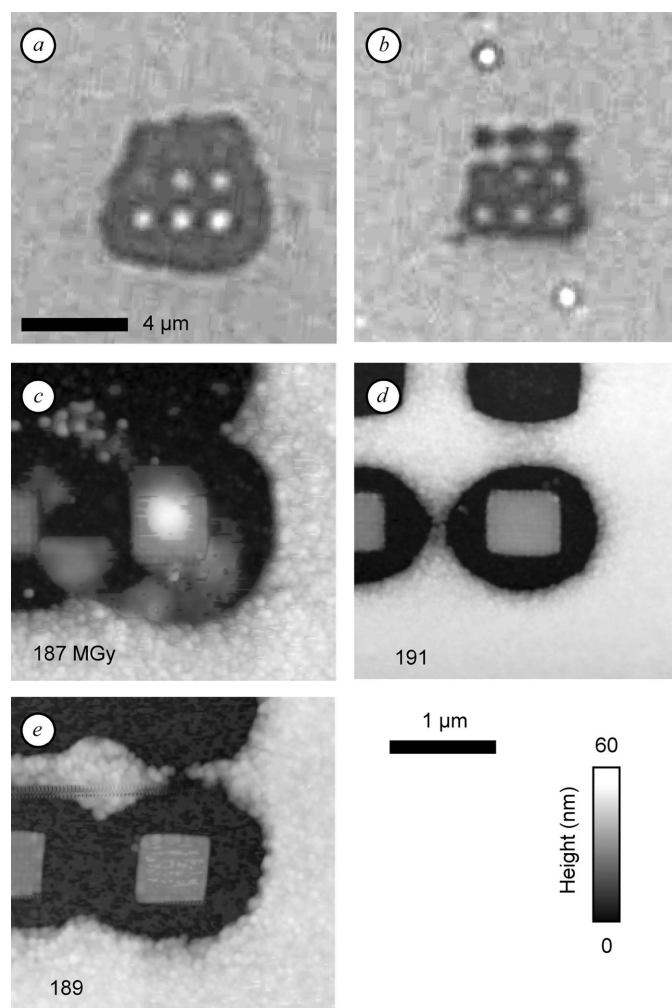
Figure 6
Optical micrographs (reflection, 100×) of developed (*a*) as-spun and (*b*) annealed (423 K, 1 h) samples, patterned with identical doses (20, 40, 59, 99, 198, 296, 395, 593, 790 MGy) and dose rates (620 MGy s^{-1}) of 300 eV X-rays [(*a*) and (*b*) are on the same spatial scale]. Atomic force micrographs of developed (*c*) as-spun, (*d*) annealed and (*e*) vacuum-dried (343 K, 2 × 10^{-2} torr, 24 h) samples which received the same dose [(*c*), (*d*) and (*e*) are on equal height and spatial scales].

observed in the area immediately surrounding the patterned areas. The mechanism of the increased lateral removal of resist beyond the presumed exposure area with increasing dose was previously identified as resulting from the point spread function of the optical system (Leontowich & Hitchcock, 2011; Leontowich *et al.*, 2011). However, given identical dose, the lateral distance beyond the patterned area over which material was removed by development was significantly greater for the as-spun and vacuum-dried samples (Fig. 6*a*) compared with annealed samples (Fig. 6*b*). Identically patterned areas were inspected by AFM (Figs. 6*c*–6*e*) for each of the sample types. The as-spun samples showed the most extensive lateral removal. The edges of the two non-annealed films are much rougher and seem to show the presence of spherical PMMA aggregates 80–100 nm in diameter. Similar PMMA aggregates or nodules have been observed previously using AFM (Dobisz *et al.*, 1997). The annealed film showed the lowest lateral

removal, smoother edges and smaller aggregates. These behaviors were independent of dose rate over the 73–1230 MGy s^{-1} range investigated.

4. Discussion

4.1. Thickness decrease

Several reports have shown that PMMA undergoes a change in height in response to dose. Here, the height of PMMA was observed to decrease with increasing dose, but only until 60 ± 15 MGy where the rate of thinning drops to zero. A decrease in film height with dose has been reported previously with soft X-rays (Zhang *et al.*, 1995) and other radiation sources including electron (Dobisz *et al.*, 1997) and ion beams. Schrempel & Witthuhn (1997) reported a linear dependence of the thickness on ion (H^{+}, He^{+}) fluence. The samples used were 1.5 mm thick, and the maximum decrease in height observed was only 1 μm, less than 1% of the virgin film height. Using ion (^{15}N^{+}) fluences two orders of magnitude larger than those of Schrempel & Witthuhn (1997), Kallweit *et al.* (1991) observed an initial linear height decrease with fluence, and no further decrease beyond a certain fluence. Schrempel *et al.* (2002) reported that irradiated areas of 1 mm-thick PMMA initially increased in height, before relaxing over 200 min to show a net decrease. An attempt was made to observe this process, and an increase in height of the patterned areas was observed in atomic force micrographs collected within 60 min of patterning at 10ID-1 (supplementary Fig. 3*a*). However, these patterned areas did not decrease in height after 36 days. The thickness increase observed here was later determined to be an artefact of carbon contamination.

The change in height in response to dose has been attributed to both loss of material and/or densification. When centimeter-sized blocks of PMMA were irradiated with neutrons and γ-rays, bubbles were observed in the interior, indicating trapped gaseous products, while the zone within approximately 1 mm from the surface did not show bubbling, which was ascribed to outgassing of the product molecules (Charlesby & Ross, 1953; Ross & Charlesby, 1953). Hiraoka (1977) identified many of the gas molecules given off by mass spectrometry. The thickness decrease could also involve a densification of the material. Rück *et al.* (1992) found that He^{+} ion-irradiated PMMA had an increased index of refraction and decreased thickness and attributed this to increased density, while Kallweit *et al.* (1991) concluded that the loss in height is entirely due to loss of material *via* outgassing as opposed to radiation-induced densification. Loss of material from an irradiated surface has been classified into desorption and ablation regimes (Haglund, 1996). The ablation threshold for PMMA occurs with power density levels which are at least three orders of magnitude greater than presently available at the STXMs used here (Makimura *et al.*, 2011). The desorption mechanism is most compatible with our observations; the observed reduction in thickness is likely due to the diffusion of gaseous product molecules out of the irradiated areas. This is supported by the observed decrease in the intensity of the C 1*s*

NEXAFS continuum signal with increasing dose (Fig. 3). The signal in the continuum region is proportional to the total amount of carbon, and eventually reaches a residual amount of approximately 70% of the virgin film. This decrease in continuum intensity has also been observed at room temperature in other STXM experiments (Coffey *et al.*, 2002; Wang *et al.*, 2007, 2009*a*) and transmission electron microscope electron energy-loss spectroscopy experiments (Egerton, 1980), and the same residual continuum signal value was observed by Coffey *et al.* (2002). Atomic force micrographs reveal a decrease in film height to a residual value of 60% (Fig. 2*b*), thus indicating the link between topography and spectroscopy. The same residual film height value was observed by Teh *et al.* (2003). The discrepancy between the larger height decrease relative to the amount of carbon lost could indicate a slight densification, but the contribution appears to be minor relative to outgassing of molecular fragments.

In passing, it is important to note that this height reduction of PMMA has been found by others to be temperature-dependent. This process of film thinning of PMMA (and other polymers) with dose has also been termed 'photo-etching'. There can be further removal of material, even full removal of the polymer film down to the substrate or 'self-development' if PMMA is heated during or following irradiation (Katoh & Zhang, 1998). Radiation-induced mass loss is often found to be temperature-dependent (Egerton, 1982; Beetz & Jacobsen, 2003). Here, the sample temperature was maintained at 298 ± 2 K throughout, and the temperature rise within the focal point has been experimentally determined to be <1 K for dose rates twice as high as the maximum used in this work (Leontowich & Hitchcock, 2012*a*).

4.2. Effect of annealing

Surface roughness was observed to decrease after annealing above T_g (Table 1), and the lateral extent of material removed around the patterned areas after development was found to depend upon the pre-exposure thermal treatment involved. Arjmandi *et al.* (2009) similarly reported that increased surface roughness was proportional to increased developed line-edge roughness for PMMA. Our measured value of T_g for powdered PMMA (376 K) is in agreement with other reported values [378 K (Rück *et al.*, 1997), 393 K (Kunz & Stamm, 1996)]. However, T_g has been shown to depend on film thickness, substrate and other effects (Fryer *et al.*, 2001); a value of 391 K has been reported for a film of similar thickness to the 50 ± 5 nm films used in this work (Keymeulen *et al.*, 2007). Our sample preparation temperatures were chosen with these values in mind. The temperature at which the vacuum-dried samples were heated was chosen so that the samples did not approach the lowest reported T_g that we are aware of for PMMA by tens of K. Likewise, the temperature at which the annealed samples were heated was tens of K higher than the highest literature T_g example that we are aware of, ensuring that the annealed samples passed through T_g. Furthermore, the amount of heat produced at the focal point of a STXM has

been shown experimentally to be <1 K with dose rates two times greater than those used in this work (Leontowich & Hitchcock, 2012*a*), negating unintended thermal processing during patterning.

In photolithography, polymer films are often baked above their T_g before being irradiated as this "promotes adhesion to the substrate" (Brewer, 1980), and also serves to remove residual solvent molecules trapped in the glassy polymer matrix during spin coating (Broers, 1981; Moreau, 1988). Ross & Charlesby (1953) and Hajimoto *et al.* (1965) have shown that small molecules trapped in a polymer 'glassy cage' can be released upon reaching or exceeding T_g. Residual solvent in the polymer layer has been shown to drastically increase the removal rate of PMMA during development (Greeneich, 1975). In addition, positron annihilation studies have shown that the size of physical voids within PMMA films decreases for films annealed at 423 K relative to non-annealed films (Puglisi *et al.*, 2001). Here, the combination of residual casting solvent and the greater permeation of the developer into the two non-annealed films owing to the increased void size increases the development rate, leading to greater lateral removal.

4.3. Critical dose

Several critical dose values for PMMA have been reported in the literature. Previous STXM measurements of the critical dose, specifically of the decrease in the C $1s$(C=O) $\rightarrow \pi^*_{C=O}$ (288.4 eV) intensity, which are directly comparable with those measured in this report, include 69.4 MGy (Coffey *et al.*, 2002), 50.0 ± 3.0 MGy (Zhang *et al.*, 1995), 13.1 ± 0.2 MGy (Zhang *et al.*, 1995), 15.2 ± 1.4 MGy (Zhang *et al.*, 1995), 67 ± 10 MGy (Wang *et al.*, 2009*a*) and 60 ± 8 MGy (Wang *et al.*, 2007). A critical dose value for C=O loss measured at the O $1s$ absorption edge could be considered to be related (Beetz & Jacobsen, 2003). The possibility of a dose-rate dependence for the critical dose for PMMA has been discussed in prior STXM work (Coffey *et al.*, 2002; Wang *et al.*, 2009*a*) but never systematically investigated to our knowledge. Room-temperature measurements of mass-loss critical doses for PMMA in electron microscopes showed no evidence of dose-rate dependence (Egerton, 1980). The critical dose measured here (62 ± 8 MGy) was found to be independent of dose rate (Fig. 4), and the highest dose rate used here (1230 MGy s^{-1}) is significantly greater than those used in all previous STXM studies [three times higher than Wang *et al.* (2009*a*)]; therefore dose rate is not a significant cause of the variability in critical doses reported in the literature.

Zhang *et al.* (1995) reported that pre-exposure thermal treatments affect the critical dose of PMMA, and their three reported critical doses correspond to three different thermal treatments: 50 ± 3 MGy (as-spun), 13.1 ± 0.2 MGy (423 K, 2 h), 15.2 ± 1.4 MGy (473 K, 2 h). In contrast, we did not observe any change in the critical dose between our as-spun, vacuum-dried and annealed (423 K, 1 h) samples. The annealing temperature may be a factor. Reported T_d values vary from as low as 443 K for a 65 nm film (Hutchings *et al.*,

2001) to 523 K for a 1 µm film (Fragalà *et al.*, 1999). Like T_g, T_d depends on many factors, including the method of polymerization and the sample thickness (Manring, 1989). It would seem possible that the sample annealed at 473 K in the Zhang *et al.* (1995) report may have partly degraded during the annealing process as this temperature is above some reported values for T_d, and could explain why it's critical dose was significantly lower. While this might explain that particular sample, there is more than a factor of four difference between the critical dose determined here and that reported by Zhang *et al.* (1995) for PMMA films annealed at 423 K. This temperature is well below the T_d measured for the as-received PMMA, and tens of K below the lowest reported T_d that we are aware of.

In the Zhang *et al.* (1995) study the critical dose for the as-spun sample was determined to be 50 MGy, yet the maximum dose administered appears to be only 30 MGy. The residual C=O bond concentration may not have been experimentally determined, and the extrapolated values may not be correct. An additional conflict is present in the data that Zhang *et al.* (1995) used to calculate the critical doses: mass loss, measured by the decrease in the C 1s NEXAFS continuum region (317 eV), was 80–100% of the original film thickness after receiving 30 MGy, indicating almost complete film loss. The C=O peak should have correspondingly decreased by an equal or greater amount, yet the C=O peak intensity decreased by only 30–40% for the same dose. Zhang *et al.* (1995) indicated that ''baked PMMA will have less cross-linking than unbaked PMMA for a given dose''. However, this was only an extrapolation from the NEXAFS data and cross-linking was not directly observed. Here we have observed the cross-linked material *via* atomic force micrographs after development and found that the amount of cross-linked material depends on dose, independent of pre-exposure thermal treatments (Fig. 5).

Two highly probable and potentially significant contributions to the variation in critical dose are (i) differences in the data collection method between studies, and (ii) detector efficiency (§4.5). The STXM measurements of Coffey *et al.* (2002) and Zhang *et al.* (1995) involved an exposure–monitor sequence; alternatively exposing the same sample area to a high dose and then interrogating that area with a low dose. In those studies only the high-dose exposure was counted. In Coffey *et al.* (2002) the interrogation was single energy images, while for Zhang *et al.* (1995) it involved recording a defocused C 1s NEXAFS spectrum. In effect, the sample received a larger dose than reported, which would make the critical dose appear lower. In contrast, Wang *et al.* (2009*a*) patterned multiple virgin areas over a range of doses, and imaged them once at a single photon energy to collect the data necessary to determine the critical dose (Fig. 4).

4.4. Detector calibration in STXM with PMMA

The decrease in film height, the critical dose for C=O loss measured at 288.4 eV, and the onset of negative mode were all found to depend on dose, independent of dose rate and pre-exposure thermal treatments. Thus it would seem that PMMA could be a robust platform for dosimetry in STXM. In fact, PMMA-based dosimeters have been commercially available for decades (Barrett, 1982). In this section the utility of these dose-dependent responses for dosimetry in STXM are outlined.

There are several drawbacks to monitoring dose by measuring a decrease in film height. Perhaps the largest is that the STXM chamber must be freshly cleaned. The chamber contains small partial pressures of carbonaceous molecules which decompose and build up on irradiated surfaces (Leontowich & Hitchcock, 2012*b*). The measurements for Fig. 2 were made using 5.3.2.2 days after it underwent a thorough cleaning process (disassemble, plasma clean, solvent rinse, reassemble, align). The rate of carbon contamination on the sample was below a measurable level for doses up to 900 MGy. However, when the nine area exposures were made at 10ID-1, the height of the patterned areas initially decreased with dose, and then increased, eventually exceeding the virgin film height (supplementary Fig. 3*a*). The growth in this case was due to carbon contamination on the sample. The carbon contamination layer could also prevent fragment molecules from escaping the patterned area, further increasing the height. Cleaning the chamber takes several days and unfortunately it does not take long for the STXM chamber to be re-polluted since the chamber is often vented to atmosphere, samples are mounted with double-sided tape and epoxy, and many samples containing volatile organics are studied. This approach also requires access to an AFM.

The radiation-induced decrease in the C $1s$(C=O) $\rightarrow \pi^*_{C=O}$ transition (288.4 eV) of PMMA and the critical dose derived from that data could be used for dosimetry. Coffey *et al.* (2002) standardized the response of multiple copies of a gas proportional counter detector for STXM relative to the radiation-induced exponential decay of the intensity of the C $1s$(C=O) $\rightarrow \pi^*_{C=O}$ peak of polycarbonate. The critical dose measurement requires identification of the residual bond concentration, and in practice this value must be decided by the observer which can be somewhat subjective. Carbon contamination, which over time causes the C 1s NEXAFS signal to increase (supplementary Fig. 3*b*), can mask the true residual bond concentration. This is problematic for critical dose measurements of radiation-resistant materials (Wang, 2008). To accurately measure the residual bond concentration for PMMA which we observe around 300 MGy, the chamber must be clean. The usefulness of critical dose as a monitor of radiation damage rates has been criticized (Cosslett, 1978). However, its application in STXM dosimetry does not require any additional equipment to measure, the data can be acquired rapidly, and the sample can remain in the chamber after the data are collected. In our view this is not the most accurate method, but it can serve as a 'quick and dirty' dosimeter to gain a fair estimate with relatively little effort.

Under the conditions used here, the dose for the onset of negative mode is exceptionally precise, within 5%. The onset occurs at 90 ± 4 MGy, which is below the point where significant carbon contamination occurred for all STXMs used

here. Identifying the onset of negative mode does require keeping the development chemicals on hand, but these are inexpensive, stable, of low hazard, and only small volumes (<10 ml) are needed per sample. The development procedure is simple, and the onset can be observed in an optical microscope equipped with a 50× or 100× objective, which most facilities have adjacent to the STXM for pre-characterization of samples.

4.5. Determination of detector efficiency using the onset of cross-linking dose

In order to compute dose, the detector efficiency must be known [equation (1)]. This value was recently measured at 5.3.2.2. However, at the other STXMs (except UE46) the detector efficiency was not known or had not been measured for some time. For most users this is not an issue as the primary use of STXMs is to collect images and X-ray absorption spectra; for these purposes it is not necessary to know the values of detector efficiency or dose. However, it is good practice to record an additional image at a damage-sensitive photon energy after any exposure-intensive measurement (*e.g.* a long stack) to check for excessive radiation damage. If the additional damage check image appears the same or only slightly different from an image recorded prior to the extensive analytical measurement, then the dose involved can be deemed acceptable (Wang *et al.*, 2009*a*). Such a check does not require that the dose be known, only that it did not significantly compromise the measurement.

The onset of negative mode at 300 eV was measured at 5.3.2.2, 11.0.2, 10ID-1, X07DA and UE46. Identical annealed samples and development procedures were used for these experiments. In each experiment the I_0 values were recorded, nine area patterns were executed with various dwell times, and the exposure time for the onset of negative mode was identified from an atomic force micrograph of the developed sample. The dose was then calculated with the assumption that the detector efficiencies at 300 eV at all STXMs were identical to that measured at 5.3.2.2. Under this assumption the dose values at which the onset of negative mode occurred differed among the various STXMs by more than an order of magnitude. Given the constant sample development conditions, dose rate and polarization independence, and that PMMA has been used as a stable and accurate dosimeter in other applications for over 40 years, an assumption was made that the dose for the onset of negative mode at 300 eV is an intrinsic value. Equation (1) was rearranged to solve for detector efficiency with 90 MGy as the value of D. The values for the detector efficiency at all the STXMs were then calculated based on this method (Table 2). In a separate and independent study, the efficiency of the avalanche photodiode detector at UE46 had been recently determined to be 4% at 300 eV by calibration against a GaAs photodiode [G1127-04, Hamamatsu (Weigand, 2012)]. With no prior knowledge of that measurement, the value obtained by our PMMA-based method matched the value determined by the photodiode method, confirming the validity of this approach.

Table 2
Measured detector efficiency (K) at 300 eV for various STXMs (measurements made between October 2010 and December 2011).

STXM	K (%)
5.3.2.2	35
11.0.2	10
10ID-1	74
X07DA	1.2
UE46	4.0

There could be several reasons why detector efficiency can differ between otherwise similar scintillator-PMT detectors. Different scintillator materials used in this application have different properties (Fakra *et al.*, 2004), and the length and face smoothness of the Lucite tubes may not be equal. Although the detectors were centered on the optical axis and the active area accepted the full bright-field signal, the detector-to-sample distance could differ by as much as 1.5 mm. However, this is expected to have a negligible effect on the detector efficiency measurements as the transmission of 300 eV X-rays through 1.5 mm of 250 torr He used in these experiments is 97.7% (Henke *et al.*, 1993). The detector, like the sample, experiences carbon contamination which degrades its performance over time. The scintillator can be contaminated and/or physically damaged by accidental contact while mounting samples. At 5.3.2.2 the scintillator is changed on a regular basis (~annually). However, the detector efficiency at 5.3.2.2 has been measured several times by our onset of negative mode method over the last three years and at 11.0.2 over the last year. The detector efficiency at each STXM had not changed significantly during those periods even though the scintillator coatings had been replaced numerous times and there were significant changes in the beamline intensity for otherwise standard slit settings, owing to changes in the storage ring and beamline optics. Nevertheless, detector efficiency values are likely to be subject to change over time. Uncertainty in the measurement of the detector efficiency is a likely reason why the critical doses for the same polymer measured in different STXMs do not match.

The common method of determining the detector efficiency of a STXM is by comparing the response of an uncharacterized detector with that of a calibrated photodiode. With current STXM designs this requires exchanging detectors which is disruptive and time-consuming; therefore the onset of the negative mode method could be an attractive complement. PMMA films are easy to make, cheap and stable for long periods of time: a time delay as long as two months between dosing and development did not affect the results, and two-year-old samples stored in a laboratory drawer in gelatin capsules gave consistent results. PMMA is insensitive to visible light [$\lambda \geq 260$ nm (Lin, 1975)]. Although M_{w} and M_{n} have not been found to affect the radiation sensitivity of PMMA (Broers, 1988), variations in M_{w} and M_{n} do affect the development characteristics. M_{w} values of less than 5×10^5 but greater than 5×10^4 g mol^{-1} show ideal overall performance (Dobisz *et al.*, 2000). Ideally, annealed samples with the same M_{w} as that used in this work should be used.

research papers

In this report several factors which were thought to affect the sensitivity of PMMA were investigated, but we cannot rule out the possible existence of other factors. A photon energy dependence has been discussed in the literature (Coffey *et al.*, 2002; Beetz & Jacobsen, 2003). Radiation sensitivity may be different below the first core ionization level (where the decay of the primary electronic excited states is *via* direct processes) relative to above the core edge, where the two-electron Auger process dominates the core hole decay (Egerton *et al.*, 2004). However, Fujii & Yokoya (2009) irradiated DNA thin films at photon energies of 395, 408, 528 and 538 eV and found no effect on the damage yields. Some of the published critical doses for PMMA were measured at damage energies different than the 300 eV chosen here. Experiments are currently underway to determine the effect of photon energy variation on the radiation sensitivity of polymers.

5. Conclusions

Several factors which were thought to affect critical dose for radiation damage to PMMA at 300 eV were tested including pre-exposure thermal treatments, dose rate and X-ray polarization. None affected quantitative aspects (increase or decrease in spectral signals and chemical change for a given dose). Some qualitative effects did depend on pre-exposure thermal treatments. The most significant sources of dose quantitation error in prior work appear to be the method in which the doses are measured and inadequate characterization of detector efficiency. The onset of negative mode (cross-linking) was found to be very reproducible and easily measured. Measurement of the exposure needed to initiate negative mode is proposed as a simple and accurate means to calibrate detector efficiency and thus establish reliable dose and dose-rates scales in STXMs.

Note added in proof. PMMA also has a positive mode (*i.e.* full removal of PMMA from the irradiated area after development) threshold dose, which was previously determined to be 1 MGy (Leontowich & Hitchcock, 2011). Very recently, we performed a detector efficiency measurement at the ALS STXM 5.3.2.1 using the positive mode threshold dose and the method described in §4.5. The efficiency of the 5.3.2.1 scintillator-PMT detector was found to be 100% at 1 keV. The positive mode threshold dose was not as precise (within 10–15%) as the negative mode threshold dose (within 5%).

References

Ade, H. & Hitchcock, A. P. (2008). *Polymer*, **49**, 643–675.
Arjmandi, N., Lagae, L. & Borghs, G. (2009). *J. Vac. Sci. Technol. B*, **27**, 1915–1918.
Barrett, J. H. (1982). *Int. J. Appl. Radiat. Isot.* **33**, 1177–1187.
Beetz, T. & Jacobsen, C. (2003). *J. Synchrotron Rad.* **10**, 280–283.
Brewer, G. R. (1980). *Electron-Beam Technology in Microelectronic Fabrication*, p. 219. New York: Academic Press.
Broers, A. N. (1981). *J. Electrochem. Soc.* **128**, 166–170.
Broers, A. N. (1988). *IBM J. Res. Dev.* **32**, 502–513.
Charlesby, A. & Ross, M. (1953). *Nature (London)*, **171**, 1153.
Coffey, T., Urquhart, S. G. & Ade, H. (2002). *J. Electron Spectrosc. Relat. Phenom.* **122**, 65–78.
Cosslett, V. E. (1978). *J. Microsc.* **113**, 113–129.
Dobisz, E. A., Brandow, S. L., Bass, R. & Mitterender, J. (2000). *J. Vac. Sci. Technol. B*, **18**, 107–111.
Dobisz, E. A., Brandow, S. L., Snow, E. & Bass, R. (1997). *J. Vac. Sci. Technol. B*, **15**, 2318–2322.
Egerton, R. F. (1980). *Ultramicroscopy*, **5**, 521–523.
Egerton, R. F. (1982). *J. Microsc.* **126**, 95–100.
Egerton, R. F., Li, P. & Malac, M. (2004). *Micron*, **35**, 399–409.
Fakra, S., Kilcoyne, A. L. D. & Tyliszczak, T. (2004). *AIP Conf. Proc.* **705**, 973–976.
Follath, R., Schmidt, J. S., Weigand, M. & Fauth, K. (2010). *AIP Conf. Proc.* **1234**, 323–326.
Fragalà, M. E., Compagnini, G. & Puglisi, O. (1999). *J. Mater. Res.* **14**, 228–231.
Frommherz, U., Raabe, J., Watts, B., Stefani, R. & Ellenberger, U. (2010). *AIP Conf. Proc.* **1234**, 429–432.
Fryer, D. S., Peters, R. D., Kim, E. J., Tomaszewski, J. E., Pablo, J. J., Nealey, P. F., White, C. C. & Wu, W. (2001). *Macromolecules*, **34**, 5627–5634.
Fujii, K. & Yokoya, A. (2009). *Radiat. Phys. Chem.* **78**, 1188–1191.
Greeneich, J. S. (1975). *J. Electrochem. Soc.* **122**, 970–976.
Haglund, R. F. Jr (1996). *Appl. Surf. Sci.* **96–98**, 1–13.
Hajimoto, Y., Tamura, N. & Okamoto, S. (1965). *J. Polym. Sci. A*, **3**, 255–263.
Hall, E. J. & Giaccia, A. J. (2006). *Radiobiology for the Radiobiologist*, 6th ed. Philadelphia: Lippincott Williams and Wilkins.
Henke, B. L., Gullikson, E. M. & Davis, J. C. (1993). *At. Data Nucl. Data Tables*, **54**, 181–342.
Hiraoka, H. (1977). *IBM J. Res. Dev.* **21**, 121–130.
Hitchcock, A. P. (2012). *Handbook of Nanoscopy*, Vol. 2, edited by G. V. Tendeloo, D. V. Dyck and S. J. Pennycook, ch. 22. New York: Wiley.
Howells, M., Jacobsen, C. & Warwick, T. (2007). *Science of Microscopy*, Vol. 2, ch. 13, edited by P. W. Hawkes and J. C. H. Spence. New York: Springer Science + Business Media.
Hubbell, J. H., Gimm, H. A. & Øverbø, I. (1980). *J. Phys. Chem. Ref. Data*, **9**, 1023–1147.
Hutchings, I. R., Richards, R. W., Thompson, R. L., Clough, A. S. & Langridge, S. (2001). *J. Polym. Sci. B*, **39**, 2351–2362.
Jacobsen, C., Wirick, S., Flynn, G. & Zimba, C. (2000). *J. Microsc.* **197**, 173–184.
Jiang, N. & Spence, J. C. H. (2012). *Ultramicroscopy*, **113**, 77–82.

Kallweit, R., Baur, M., Eichinger, P. & Strack, H. (1991). *Nucl. Instrum. Methods Phys. Res. B*, **59/60**, 1288–1291.

Katoh, T. & Zhang, Y. (1998). *J. Synchrotron Rad.* **5**, 1153–1156.

Kaznatcheev, K. V., Karunakaran, Ch., Lanke, U. D., Urquhart, S. G., Obst, M. & Hitchcock, A. P. (2007). *Nucl. Instrum. Methods Phys. Res. A*, **582**, 96–99.

Keymeulen, H. R., Diaz, A., Solak, H. H., David, C., Pfeiffer, F., Patterson, B. D., Veen, J. F., Stoykovich, M. P. & Nealey, P. F. (2007). *J. Appl. Phys.* **102**, 013528.

Kilcoyne, A. L. D. & Tyliszczak, T. (2004). *AIP Conf. Proc.* **705**, 605–607.

Kilcoyne, A. L. D., Tyliszczak, T., Steele, W. F., Fakra, S., Hitchcock, P., Franck, K., Anderson, E., Harteneck, B., Rightor, E. G., Mitchell, G. E., Hitchcock, A. P., Yang, L., Warwick, T. & Ade, H. (2003). *J. Synchrotron Rad.* **10**, 125–136.

King, M. C. & Laidler, K. J. (1984). *Arch. Hist. Exact Sci.* **30**, 45–86.

Kunz, K. & Stamm, M. (1996). *Macromolecules*, **29**, 2548–2554.

Leiros, H.-K. S., Timmins, J., Ravelli, R. B. G. & McSweeney, S. M. (2006). *Acta Cryst.* D**62**, 125–132.

Leontowich, A. F. G. & Hitchcock, A. P. (2011). *Appl. Phys. A*, **103**, 1–11.

Leontowich, A. F. G. & Hitchcock, A. P. (2012*a*). *Analyst*, **137**, 370–375.

Leontowich, A. F. G. & Hitchcock, A. P. (2012*b*). *J. Vac. Sci. Technol. B*, **30**, 030601.

Leontowich, A. F. G., Tyliszczak, T. & Hitchcock, A. P. (2011). *Proc. SPIE*, **8077**, 80770N.

Lin, B. J. (1975). *J. Vac. Sci. Technol.* **12**, 1317–1320.

Makimura, T., Torii, S., Okazaki, K., Nakamura, D., Takahashi, A., Niino, H., Okada, T. & Murakami, K. (2011). *Proc. SPIE*, **8077**, 80770F.

Manring, L. E. (1989). *Macromolecules*, **22**, 2673–2677.

Moreau, W. M. (1988). *Semiconductor Lithography: Principles, Practices and Materials*, ch. 7. New York: Plenum Press.

Plaček, V., Bartoníček, B., Hnát, V. & Otáhal, B. (2003). *Nucl. Instrum. Methods Phys. Res. B*, **208**, 448–453.

Puglisi, O., Fragalà, M. E., Lynn, K. G., Petkov, M., Weber, M., Somoza, A., Dupasquier, A. & Quasso, F. (2001). *Nucl. Instrum. Methods Phys. Res. B*, **175–177**, 605–609.

Raabe, J., Tzvetkov, G., Flechsig, U., Böge, M., Jaggi, A., Sarafimov, B., Vernooij, M. G., Huthwelker, T., Ade, H., Kilcoyne, D., Tyliszczak, T., Fink, R. H. & Quitmann, C. (2008). *Rev. Sci. Instrum.* **79**, 113704.

Ross, M. & Charlesby, A. (1953). *Atom. Atom. Tech.* **4**, 189–194.

Rück, D. M., Brunner, S., Frank, W., Kulisch, J. & Franke, H. (1992). *Surf. Coatings Tech.* **51**, 318–323.

Rück, D. M., Schulz, J. & Deusch, N. (1997). *Nucl. Instrum. Methods Phys. Res. B*, **131**, 149–158.

Schrempel, F., Kim, Y. & Witthuhn, W. (2002). *Appl. Surf. Sci.* **189**, 102–112.

Schrempel, F. & Witthuhn, W. (1997). *Nucl. Instrum. Methods Phys. Res. B*, **132**, 430–438.

Teh, W. H., Liang, C., Graham, M. & Smith, C. G. (2003). *J. Microelectromech. Sys.* **12**, 641–648.

Tyliszczak, T., Warwick, T., Kilcoyne, A. L. D., Fakra, S., Shuh, D. K., Yoon, T. H., Brown, G. E. Jr, Andrews, S., Chembrolu, V., Strachan, J. & Acremann, Y. (2004). *AIP Conf. Proc.* **705**, 1356–1359.

Wang, J. (2008). *Radiation Chemistry by Soft X-ray Spectromicroscopy*, Appendix A. Hamilton: McMaster University.

Wang, J., Botton, G. A., West, M. M. & Hitchcock, A. P. (2009*b*). *J. Phys. Chem. B*, **113**, 1869–1876.

Wang, J., Morin, C., Li, L., Hitchcock, A. P., Scholl, A. & Doran, A. (2009*a*). *J. Electron Spectrosc. Relat. Phenom.* **170**, 25–36.

Wang, J., Stöver, H. D. H., Hitchcock, A. P. & Tyliszczak, T. (2007). *J. Synchrotron Rad.* **14**, 181–190.

Weigand, M. (2012). In preparation.

Zhang, X., Jacobsen, C., Lindaas, S. & Williams, S. (1995). *J. Vac. Sci. Technol. B*, **13**, 1477–1483.